Nucleon Axial and Electromagnetic Form Factors from 2+1+1-flavor QCD

Yong-Chull Jang

BROOKHAVEN NATIONAL LABORATORY

(PNDME Collaboration)

The 37th International Symposium on Lattice Field Theory

Lattice 19

Wuhan·China | June 16-22

Outline

1. A possible cure for the PCAC puzzle and impacts on axial form factors

   [arXiv:1905.06470]

2. Various systematics in calculation of nucleon EM form factors

   [arXiv:1906.07217]

Lattice Methodology

Ensemble ID	a (fm)	$M_\pi^{\rm sea}$ (MeV)	$M_\pi^{\rm val}$ (MeV)	$L^3 \times T$	$M_\pi^{\rm val} L$	τ/a	$N_{\rm conf}$	$N_{\rm meas}^{\rm HP}$	$N_{\rm meas}^{\rm LP}$
$a15m310$	0.1510(20)	306.9(5)	320(5)	$16^3 \times 48$	3.93	$\{5,6,7,8,9\}$	1917	7668	122,688
$a12m310$	0.1207(11)	305.3(4)	310.2(2.8)	$24^3 \times 64$	4.55	$\{8,10,12\}$	1013	8104	64,832
a12m220S	0.1202(12)	218.1(4)	225.0(2.3)	$24^3 \times 64$	3.29	$\{8,10,12\}$	946	3784	60,544
a12m220	0.1184(10)	216.9(2)	227.9(1.9)	$32^3 \times 64$	4.38	$\{8,10,12\}$	744	2976	47,616
a12m220L	0.1189(09)	217.0(2)	227.6(1.7)	$40^3 \times 64$	5.49	$\{8,10,12,14\}$	1000	4000	128,000
$a09m310$	0.0888(08)	312.7(6)	313.0(2.8)	$32^3 \times 96$	4.51	$\{10,12,14,16\}$	2263	9052	144,832
$a09m220$	0.0872(07)	220.3(2)	225.9(1.8)	$48^3 \times 96$	4.79	$\{10,12,14,16\}$	964	7712	123,392
a09m130W	0.0871(06)	128.2(1)	138.1(1.0)	$64^3 \times 96$	3.90	$\{8,10,12,14,16\}$	1290	5160	165,120
$a06m310$	0.0582(04)	319.3(5)	319.6(2.2)	$48^3 \times 144$	4.52	$\{16,20,22,24\}$	1000	8000	64,000
a06m310W						$\{18,20,22,24\}$	500	2000	64,000
$a06m220$	0.0578(04)	229.2(4)	235.2(1.7)	$64^3 \times 144$	4.41	$\{16,20,22,24\}$	650	2600	41,600
a06m220W						$\{18,20,22,24\}$	649	2596	41,536
$a06m135$	0.0570(01)	135.5(2)	135.6(1.4)	$96^3 \times 192$	3.7	$\{16,18,20,22\}$	675	2700	43,200

- Clover on the $N_f = 2+1+1$ HISQ Ensembles generated by MILC collaboration
- different volumes for the same pion mass and lattice spacing
- "W": covariant gaussian smearing with larger width
- High statistics data at $a = 0.09$ fm
- truncated solver method with bias correction for all τ/a

- Thanks for computing allocations to NERSC, OLCF, USQCD, and LANL IC

Nucleon Axial Form Factors

Axial Form Factor Decomposition

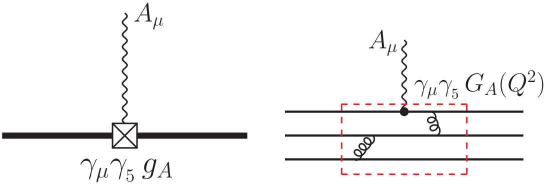

- form factors for axial $A_\mu = \bar{u}\gamma_\mu\gamma_5 d$ and pseudoscalar $P = \bar{u}\gamma_5 d$ interactions

$$\langle N(\vec{p}_f)|A_\mu(\vec{Q})|N(\vec{p}_i)\rangle = \overline{u}(\vec{p}_f)\left[G_A(Q^2)\gamma_\mu + q_\mu \frac{\widetilde{G}_P(Q^2)}{2M}\right]\gamma_5 u(\vec{p}_i)$$

$$\langle N(\vec{p}_f)|P(\vec{q})|N(\vec{p}_i)\rangle = \overline{u}(\vec{p}_f)\left[G_P(Q^2)\gamma_5\right] u(\vec{p}_i)$$

$$q = p_f - p_i,\ Q^2 = -q^2 = \vec{p}_f^{\,2} - (E-M)^2,\ \vec{p}_i = 0$$

- charge, charge radius

$$G_A(0) \equiv g_A\,, \quad \langle r_A^2\rangle = -6\frac{d}{dQ^2}\left(\frac{G_A(Q^2)}{G_A(0)}\right)\Bigg|_{Q^2=0}$$

- *isovector* current on the lattice $A_\mu^{u-d} = \bar{u}\gamma_\mu\gamma_5 u - \bar{d}\gamma_\mu\gamma_5 d$

$$\langle p|A_\mu|n\rangle = \langle p|A_\mu^{u-d}|p\rangle \quad \text{(isospin limit)}$$

Axial Form Factor $G_A(Q^2)$ and Charge Radius $\langle r_A^2 \rangle$

[Y.-C. Jang. *et. al*, PNDME, Lattice 2018]

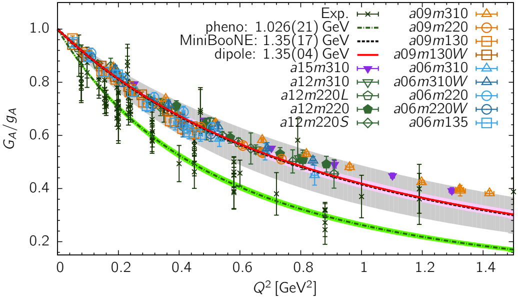

- neutrino scattering:
  $r_A = 0.666(17)\text{fm}$,
  $\mathcal{M}_A = 1.026(21)\text{GeV}$
- Deuterium:
  $r_A = 0.68(16)\text{fm}$, $\mathcal{M}_A = 1.00(24)$
  [PRD93, 113015 (2016)]

- Lattice calculation results in a smaller axial charge radius.
- 11-point extrapolation $\langle r_A^2 \rangle(a, M_\pi, M_\pi L)$:

  $r_A = 0.481(58)(62)\,\text{fm}$, $\mathcal{M}_A = 1.42(17)(18)\,\text{GeV}$ from z-expansion fit @ z^{3+4}

  $r_A = 0.505(13)(6)\,\text{fm}$, $\mathcal{M}_A = 1.35(3)(2)\,\text{GeV}$ from dipole fit

  systematic error: difference of $\langle r_A^2 \rangle$ from two physical ensembles

- Not much changes from $r_A = 0.48(4)\text{fm}$ [R. Gupta, *et. al.*(PNDME) PRD96, 114503 (2017)], although statistics is increased and data set is enlarged.

PCAC and Pion-pole Dominance

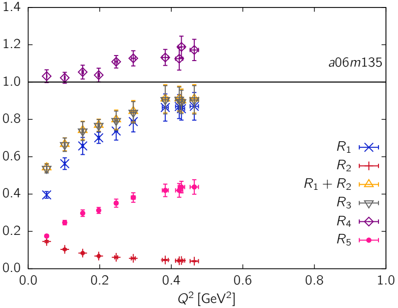

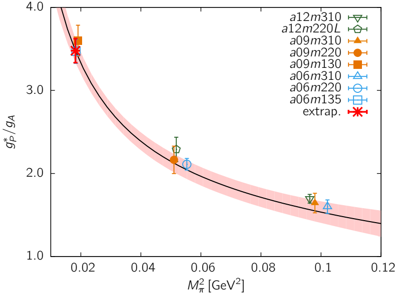

- PCAC relation ($R_1 + R_2 = 1$) is not satisfied.

$$2\widehat{m}G_P(Q^2) = 2M_N G_A(Q^2) - \frac{Q^2}{2M_N}\widetilde{G}_P(Q^2)$$

$$R_1 = \frac{Q^2}{4M_N^2}\frac{\tilde{G}_P(Q^2)}{G_A(Q^2)}, \quad R_2 = \frac{2\widehat{m}}{2M_N}\frac{G_P(Q^2)}{G_A(Q^2)}$$

- Pion-pole dominance hypothesis ($R_3 = 1$) shows a large deviation as $Q^2 \to 0$, but remains close to $R_1 + R_2$.

$$R_3 = \frac{Q^2 + M_\pi^2}{4M_N^2}\frac{\tilde{G}_P(Q^2)}{G_A(Q^2)}$$

- $\mathcal{O}(a)$ improvement of A_μ does not fix PCAC.
[R. Gupta, *et. al.*(PNDME) PRD96, 114503]

- As a consequence of lacking the pion-pole dominace, the coupling g_P^* is about 1/2 of the experimental value $(g_P^*/g_A)_{\rm exp} \sim 6.3$, $[\mu^- + p \to \nu_\mu + n]$

$$g_P^* \equiv \frac{m_\mu}{2M_N}\tilde{G}_P(0.88m_\mu^2)$$

Extracting Form Factors from 3-pt Correlators $C_\Gamma^{(3\mathrm{pt})}$

- Matrix elements $\mathcal{M}_{i'j} \equiv \langle i'|\mathcal{O}_\Gamma|j\rangle$ are extracted from a simultaneous fit to the correlator $C_\Gamma^{(3\mathrm{pt})}$ calculated at multiple τ.

$$
\begin{aligned}
C_\Gamma^{(3\mathrm{pt})}(t;\tau;\boldsymbol{p}',\boldsymbol{p}=\boldsymbol{0}) = {}& |\mathcal{A}_0'||\mathcal{A}_0|\langle 0'|\mathcal{O}_\Gamma|0\rangle e^{-E_0 t - M_0(\tau-t)} \\
&+ |\mathcal{A}_1'||\mathcal{A}_1|\langle 1'|\mathcal{O}_\Gamma|1\rangle e^{-E_1 t - M_1(\tau-t)} + |\mathcal{A}_2'||\mathcal{A}_2|\langle 2'|\mathcal{O}_\Gamma|2\rangle e^{-E_2 t - M_2(\tau-t)} \\
&+ |\mathcal{A}_0'||\mathcal{A}_1|\langle 0'|\mathcal{O}_\Gamma|1\rangle e^{-E_0 t - M_1(\tau-t)} + |\mathcal{A}_1'||\mathcal{A}_0|\langle 1'|\mathcal{O}_\Gamma|0\rangle e^{-E_1 t - M_0(\tau-t)} \\
&+ |\mathcal{A}_0'||\mathcal{A}_2|\langle 0'|\mathcal{O}_\Gamma|2\rangle e^{-E_0 t - M_2(\tau-t)} + |\mathcal{A}_2'||\mathcal{A}_0|\langle 2'|\mathcal{O}_\Gamma|0\rangle e^{-E_2 t - M_0(\tau-t)} \\
&+ |\mathcal{A}_1'||\mathcal{A}_2|\langle 1'|\mathcal{O}_\Gamma|2\rangle e^{-E_1 t - M_2(\tau-t)} + |\mathcal{A}_2'||\mathcal{A}_1|\langle 2'|\mathcal{O}_\Gamma|1\rangle e^{-E_2 t - M_1(\tau-t)} + \dots
\end{aligned}
$$

- $(\mathcal{A}_i',\ E_i)$ for proton with $\boldsymbol{p}'$ and $(\mathcal{A}_j,\ M_j)$ for proton at rest are taken from 2-pt correlator fits (4-state).
- 3^*-state fit: $\langle 2'|\mathcal{O}_\Gamma|2\rangle = 0$

- Decompose the ground state matrix elements

$$\langle 0'|\mathcal{O}_\Gamma|0\rangle = K_{A,\Gamma} G_A + K_{P,\Gamma} \widetilde{G}_P + K_{PS,\Gamma} G_P$$

Γ	$\gamma_5\gamma_1$	$\gamma_5\gamma_2$	$\gamma_5\gamma_3$	$\gamma_5\gamma_4$	γ_5
Re $C_\Gamma^{(3\mathrm{pt})}$				$q_3\{2M_0 G_A - (E_0 - M_0)\widetilde{G}_P\}$	$q_3 G_P$
Im $C_\Gamma^{(3\mathrm{pt})}$	$q_1 q_3 \widetilde{G}_P$	$-q_2 q_3 \widetilde{G}_P$	$2M_0(M_0+E_0)G_A - q_3^2 \widetilde{G}_P$		

- cannot fit A_4 with small $\boldsymbol{p}'$ to 3^*-state spectral decomposition
- ChPT including $N\pi$ state gives a large shift in $\widetilde{G}_P$ [O. Bär, PRD99, 054506 (2019)]
- spectrum from 2-pt correlator does not show $N\pi$ state.

Axial Current A_4 3-pt Correlator

[arXiv:1905.06470]

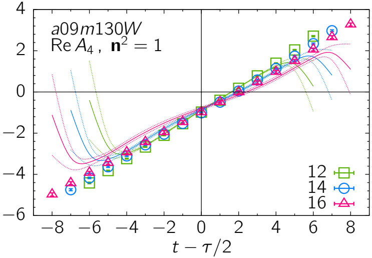

[3*-state]

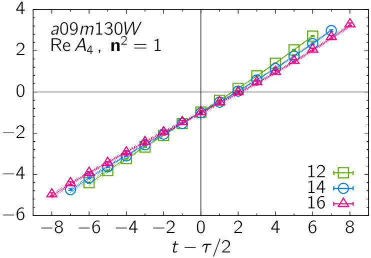

[relaxed 2-state]

- $E_i, \mathcal{A}'_i$ and $M_j, \mathcal{A}_j$ are taken from 4-state fits to nucleon two-point correlator. $(i, j = 0, 1, 2)$
- $E_0, \mathcal{A}'_0$ and $M_0, \mathcal{A}_0$ are taken from nucleon two-point correlator fits. Excited state parameters are free.

	3*-state		relaxed 2-state	
$\boldsymbol{n}^2$	χ^2/d.o.f	p-value	χ^2/d.o.f	p-value
1	21.78	$< 5 \times 10^{-5}$	0.698	0.76
2	19.36	$< 5 \times 10^{-5}$	1.654	0.06
3	11.79	$< 5 \times 10^{-5}$	2.018	0.02

Nucleon Spectrum from A_4

[arXiv:1905.06470]

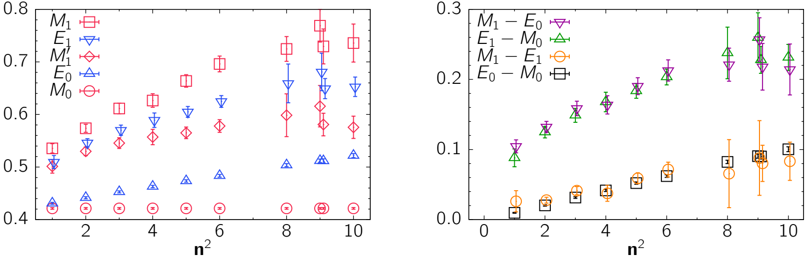

- E_1 and M_1 are extracted from the relaxed 2-state fits to $A_4(\boldsymbol{p}')$, $a\boldsymbol{p}' = 2\pi\boldsymbol{n}/L$
- The rest mass for E_1 is $M_1' = \sqrt{E_1^2 - c^2\boldsymbol{p}^2} = \sqrt{E_1^2 - E_0^2 + M_0^2}$.
- $M_1' < M_1$: $|1'\rangle$ is not connected with $|1\rangle$ by the Lorentz boost.
- $e^{(M_j - E_i)t}$ for a fixed τ: $-(M_0 - E_0) \simeq M_1 - E_1 < -(M_0 - E_1) \simeq M_1 - E_0$
- $\mathcal{M}_{i'j} = \langle i'|\mathcal{O}|j\rangle$, $r_i^{(\prime)} = |A_i^{(\prime)}|/|A_0|$.

$\boldsymbol{n}^2$	$\mathcal{M}_{0'0}$	$r_1\mathcal{M}_{0'1}$	$r_1'\mathcal{M}_{1'0}$	$r_1' r_1\mathcal{M}_{1'1}$
1	$3.35(7.62)\times10^{-1}$	4.18(59)	-6.41(67)	1.84(82)
2	$-0.27(1.39)\times10^{-2}$	3.18(14)	-4.36(08)	0.75(42)
3	$-2.11(8.88)\times10^{-3}$	2.46(12)	-3.49(08)	0.73(46)

Structure of spectrum accessed at fixed $\boldsymbol{n}^2$

[arXiv:1905.06470]

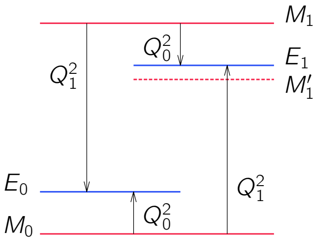

$\left(Q_i^2 = \boldsymbol{p}^2 - (E_i - M_0)^2\right)$

- Given momentum $\boldsymbol{p}'$ insertion, pion absorption and emission are paired.
  $0 \rightarrow 0'$ is paired with $1 \rightarrow 1'$ at the same Q_0^2
  $0 \rightarrow 1'$ is paired with $1 \rightarrow 0'$ at the same Q_1^2

Excited State Spectrum

[arXiv:1905.06470]

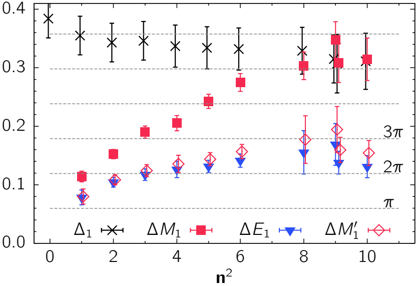

- Δ_1: energy gap for the 1st excited state, which is extracted from $C^{2\text{pt}}$.
- $\Delta M_1^{(\prime)} = M_1^{(\prime)} - M_0$, $\Delta E_1 = E_1 - E_0$, where $M_1^{(\prime)}$, E_1 are extracted from $C^{3\text{pt}}[A_4]$.
- different excited state spectrum from $C^{2\text{pt}}$ and $C^{3\text{pt}}[A_4]$
- $C^{3\text{pt}}[A_4]$ reveals that there are large number of excited states.
- $\Delta M_1'(\boldsymbol{n}^2 = 1) \sim M_\pi$ corresponds to the lowest level accessed from $C^{3\text{pt}}[A_4]$.

	$\boldsymbol{n}^2$: ΔM_1	$\boldsymbol{n}^2$: $\Delta M_1'$	
$N\pi$		1: 0.080(13)	
$(N\pi\pi)_1$	1: 0.114(09)	2: 0.108(08)	3: 0.124(10)
$(N\pi\pi)_2$	2: 0.152(08)	5: 0.144(11)	6: 0.157(12)

PCAC with Excited States from A_4

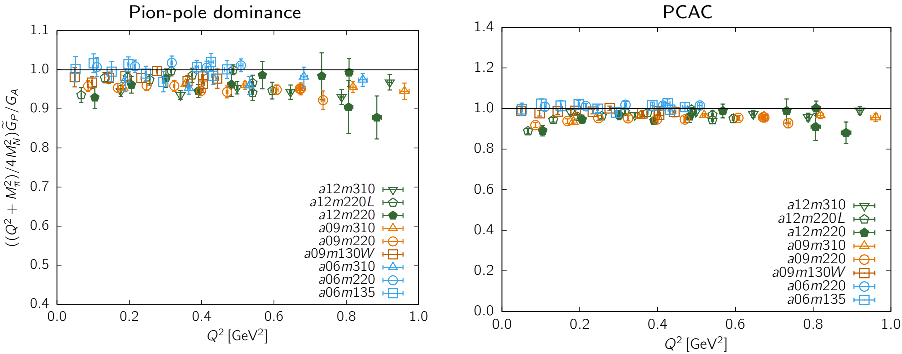

- $C^{3\text{pt}}[A_i]$ $(i = 1, 2, 3)$ and $C^{3\text{pt}}[P]$ are reanalyzed with 2-state fit using the excited states extracted from $C^{3\text{pt}}[A_4]$.
- PCAC is satisfied better for all Q^2.
- Pion-pole dominance becomes a prominent hypothesis.
- The deviation from the exact limit $(y = 1)$ diminises as $a \to 0$, $M_\pi \to 135\text{MeV}$.

$\widetilde{G}_P(Q^2)$ and g_P^* with Excited States from A_4

excited states from 2-point correlators

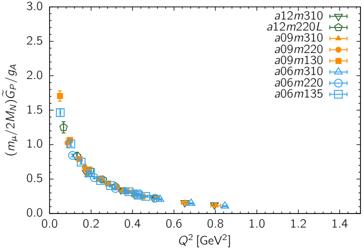

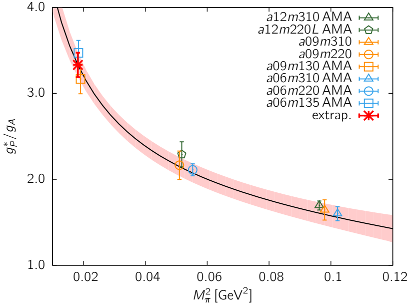

[R. Gupta, *et. al.*(PNDME) PRD96, 114503]

excited states from 3-point A_4 correlators

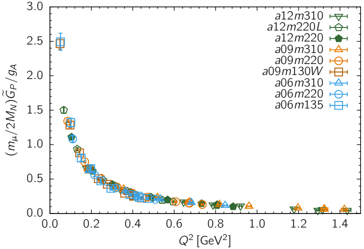

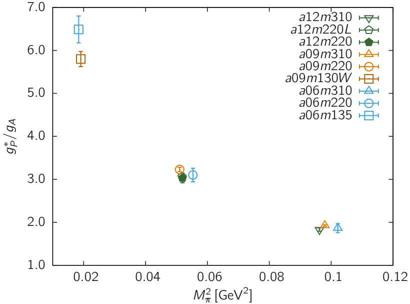

The correction in $\widetilde{G}_P$ and g_P^* is large as the $M_\pi \to 135\ \mathrm{MeV}$

$G_A(Q^2)$ with Excited States from A_4

(Fit A)

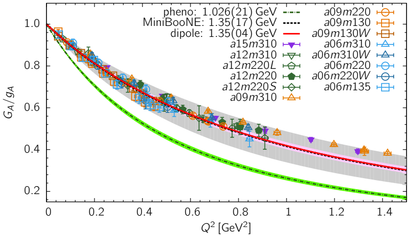

- (Fit A): 3^*-state fit. Excited states are taken from 2-point correlator fits, which include 4 states. [PNDME, Lattice 2018]
- (Fit B): 2-state fit. Reanalyze $G_A(Q^2 \neq 0)$ using excited states from A_4.
- (Fit C): 2-state fit. Reanalyze g_A using the lowest level of $\Delta M_1'$, which is derived from ΔE_1 of $A_4(\boldsymbol{n}^2 = 1)$, in addition to Fit B.
- Dipole curve represents the CCFV fit result $\langle r_A^2 \rangle$ from the lattice data in (Fit A).

(Fit B)

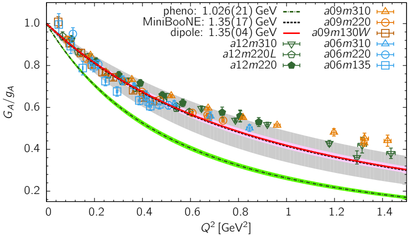

(Fit C)

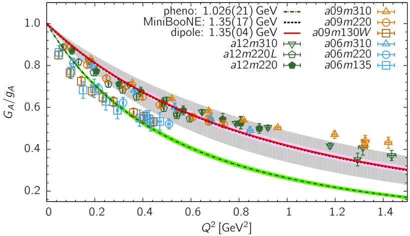

Summary (1)

- $C^{\mathrm{3pt}}[A_4]$ can be used to extract the excited states that couple to axial current A_μ.
- The PCAC is satisfied.
- Undershooting of g_P^*, $\langle r_A^2 \rangle$, g_A could be understood.
- $C^{\mathrm{3pt}}[A_4]$ vanishes at $Q^2 = 0$.
- $C^{\mathrm{3pt}}[A_4]$ with $Q^2 \neq 0$ reveals several number of excited states $\Delta M_1 \lesssim 3M_\pi$.
- Further consideration is required to treat the excited state systematics in $\langle r_A^2 \rangle$ and g_A.

Nucleon Electromagnetic Form Factors

Form Factor Decomposition

- EM form factors, charge, magnetic moment, charge radii :

$$\langle N(\vec{p}_f)|V_\mu(\vec{q})|N(\vec{p}_i)\rangle = \overline{u}(\vec{p}_f)\left[F_1(Q^2)\gamma_\mu + \sigma_{\mu\nu}q_\nu\frac{F_2(Q^2)}{2M}\right]u(\vec{p}_i)$$

$$q = p_f - p_i,\ Q^2 = -q^2 = \vec{p}_f^{\,2} - (E-M)^2,\ \vec{p}_i = 0$$

$$G_E(Q^2) = F_1(Q^2) - \frac{Q^2}{4M^2}F_2(Q^2) \to \langle r_E^2\rangle,\ G_E(0) \equiv g_V$$

$$G_M(Q^2) = F_1(Q^2) + F_2(Q^2) \qquad \to \langle r_M^2\rangle,\ G_M(0)/g_V \equiv \mu$$

$$\langle r_{E,M}^2\rangle = -6\frac{d}{dQ^2}\left(\frac{G_{E,M}(Q^2)}{G_{E,M}(0)}\right)\Bigg|_{Q^2=0}$$

- *Isovector* current $V_\mu^{u-d} = \bar{u}\gamma_\mu u - \bar{d}\gamma_\mu d$ on the lattice

$$\langle p|V_\mu^{u-d}|p\rangle = \langle p|V_\mu^{\rm em}|p\rangle - \langle n|V_\mu^{\rm em}|n\rangle$$

$$V_\mu^{\rm em} = \frac{2}{3}\bar{u}\gamma_\mu u - \frac{1}{3}\bar{d}\gamma_\mu d$$

Extraction of G_E

- $\mathrm{Re}\, C[V_4] \to q_i G_E / \sqrt{2E(E+M)}$
- $\mathrm{Re}\, C[V_4]$ converges from above: could overestimate the G_E
- G_E/g_V versus Q^2/M_N^2: all 13 calculations fall into a thin band
- Comparison to the experimental data is made with the Kelly parameterization.

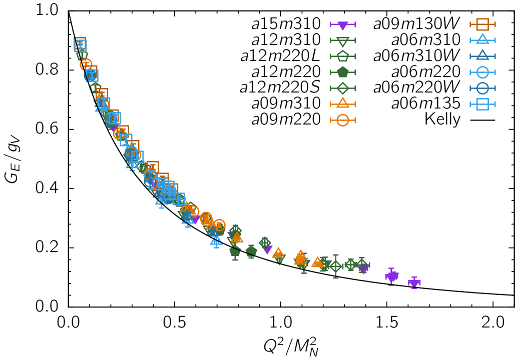

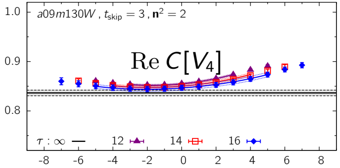

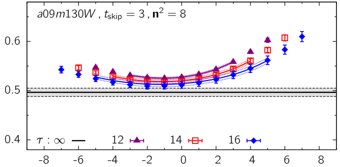

Extraction of G_M

- $\mathrm{Re}\, C[V_i] \to -\epsilon_{ij3} q_j G_M / \sqrt{2E(E+M)}$
- For the small Q^2 ($\boldsymbol{n}^2 = 1, 2$), the convergence is from below: could underestimates the G_M
  Or, a large finite volume effect at small Q^2 ?
  [B. C. Tiburzi, PRD **77**, 014510 (2008)]
- G_M/g_V versus Q^2/M_N^2:
  all 13 calculations fall into a thin band

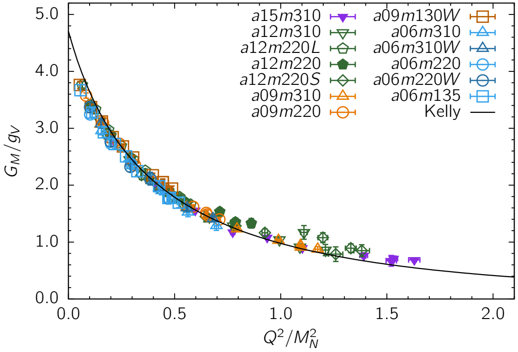

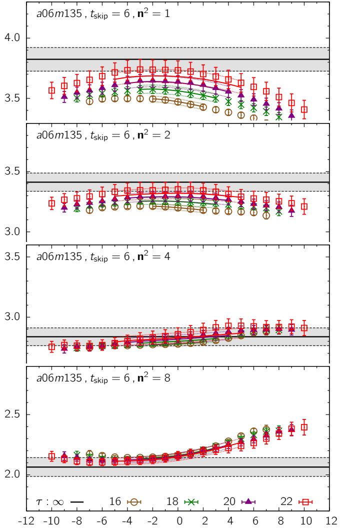

Estimate of $G_M(Q^2 = 0)$

- G_M/G_E (or G_E/G_M) for $Q^2 \lesssim 0.6\mathrm{GeV}^2$ is approximately linear in Q^2.
- $G_M(0)$: a linear fit to G_M/G_E incluing 6 (or 5 when data lacks) low Q^2 point is extrapolated to $Q^2 = 0$.
- The derived data points stabilizes the Q^2 fit, and thus extraction of charge radius r_M.

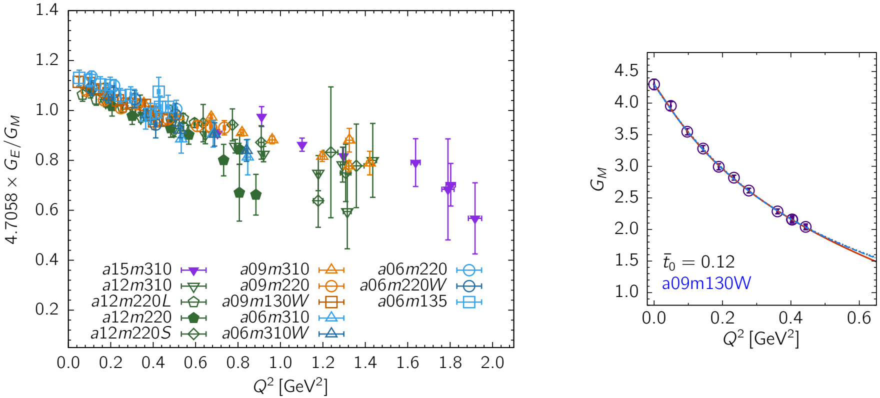

$(\mu^{p-n}_{\text{phys}} = 4.7058)$

Form Factor Q^2 Parameterization

- dipole

$$G_E(Q^2) = \frac{G_E(0)}{(1+Q^2/\mathcal{M}_E^2)^2} \quad \Longrightarrow \quad \langle r_E^2 \rangle = \frac{12}{\mathcal{M}_E^2}$$

- z-expansion

$$G_E(Q^2) = \sum_{k=0}^{\infty} a_k z(Q^2)^k \,, \; z = \frac{\sqrt{t_{\rm cut}+Q^2} - \sqrt{t_{\rm cut}+\bar{t}_0}}{\sqrt{t_{\rm cut}+Q^2} + \sqrt{t_{\rm cut}+\bar{t}_0}} \,, \; (t_{\rm cut} = 4M_\pi^2)$$

- weak unitarity constraint: a_k are bounded and decreasing at sufficiently large k

$$\sum_{k=n} a_k^2 < \infty$$

We impose a prior $|a_k| < 5$ for G_E and $G_M/5$. crucial to see a convergence

- sum rules implement $Q^n G_E(Q^2) \to 0$ for $n = 0, 1, 2, 3$: $\mathcal{O}(1/k^4)$ fall-off of a_k
strong constraint

$$\sum_{k=0}^{k_{\rm max}} a_k = 0 \,, \quad \sum_{k=n}^{k_{\rm max}} k(k-1)\ldots(k-n+1) a_k = 0 \quad (n = 1, 2, 3)$$

z-expansion

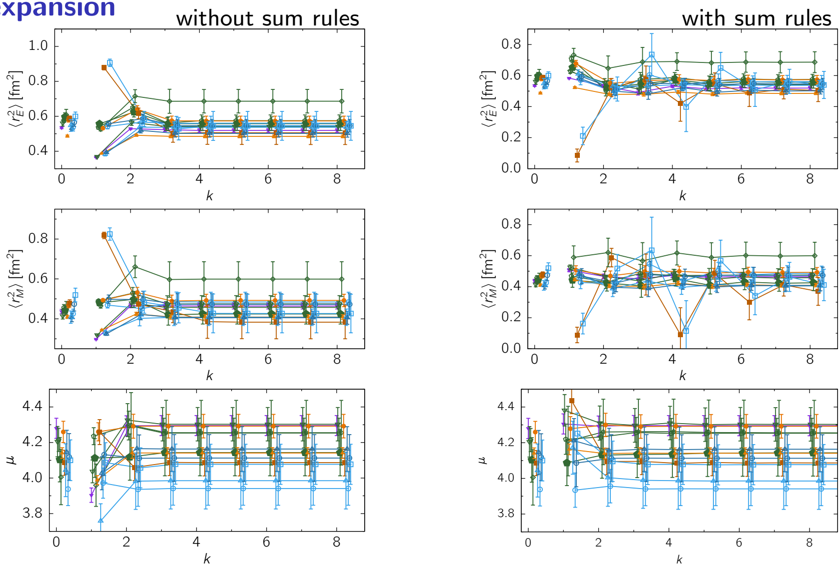

- Fits with the sum rules slowly converges. But, later it converges to the same value to the fit without the sum rules. Avoiding overfitting, we take z^4 fit.
- $k = 0$: dipole fit

- with a cutoff $Q^2 \sim 1\mathrm{GeV}^2$, we drop the data points with large discretization error.

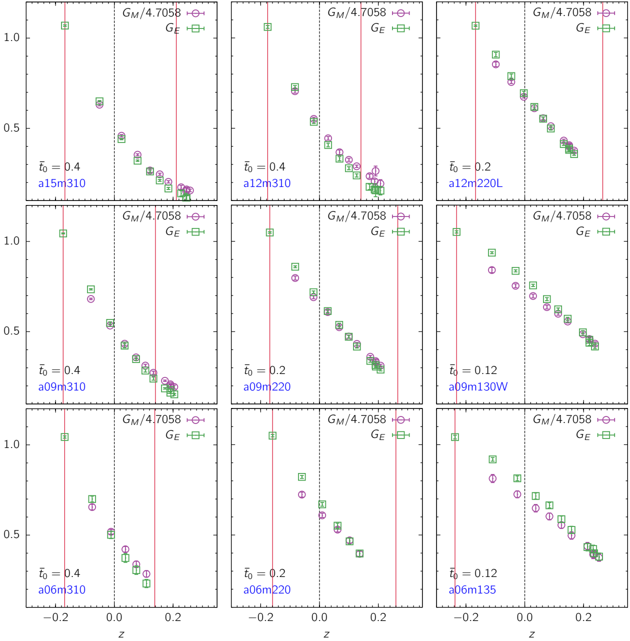

- $|z| \lesssim 0.2$

  $\bar{t}_0 \in \{0.12, 0.2, 0.4\}$

r_E^2: Chiral, Continuum, Finite Volume (CCFV) Extrapolation

$$\langle r_E^2 \rangle = c_1^E + c_2^E a + c_3^E \ln(M_\pi^2/M_\rho^2) + c_4^E \ln(M_\pi^2/M_\rho^2) e^{-M_\pi L}$$

dipole : 0.586(17)(13) fm^2 $\qquad$ z^4 : 0.591(41)(46) fm^2

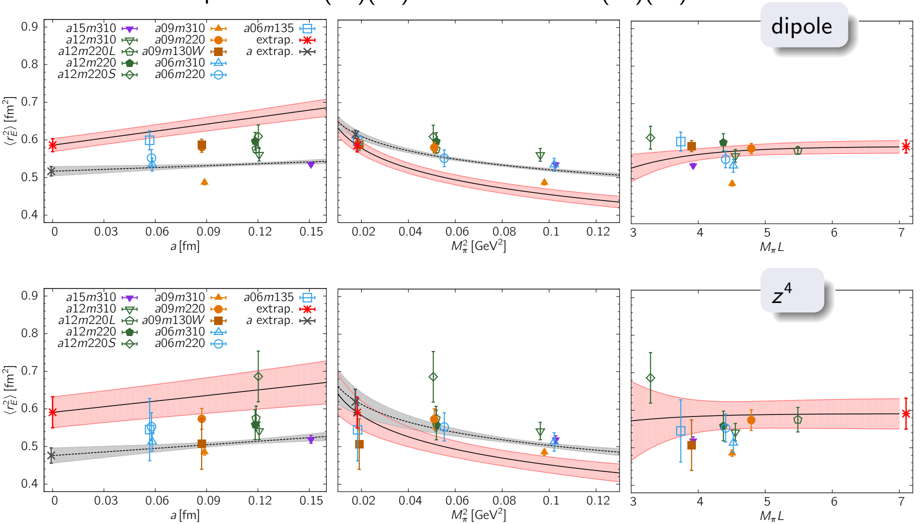

r_M^2: Chiral, Continuum, Finite Volume (CCFV) Extrapolation

$$\langle r_M^2 \rangle = c_1^M + c_2^M a + c_3^M / M_\pi + (c_4^M / M_\pi) e^{-M_\pi L}$$

dipole : $0.495(29)(41)\,\mathrm{fm}^2$ $\quad z^4$: $0.450(65)(102)\,\mathrm{fm}^2$

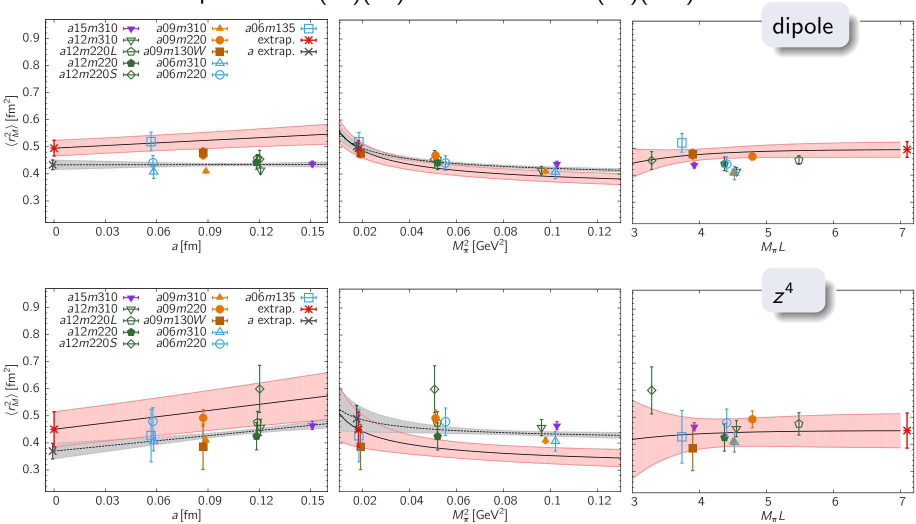

$\mu_p - \mu_n$: Chiral, Continuum, Finite Volume (CCFV) Extrapolation

$$\langle \mu \rangle = c_1^{\mu} + c_2^{\mu} a + c_3^{\mu} M_{\pi} + c_4^{\mu} M_{\pi} \left(1 - \frac{2}{M_{\pi} L}\right) e^{-M_{\pi} L}$$

dipole : 3.975(84)(125) z^4 : 3.939(86)(138)

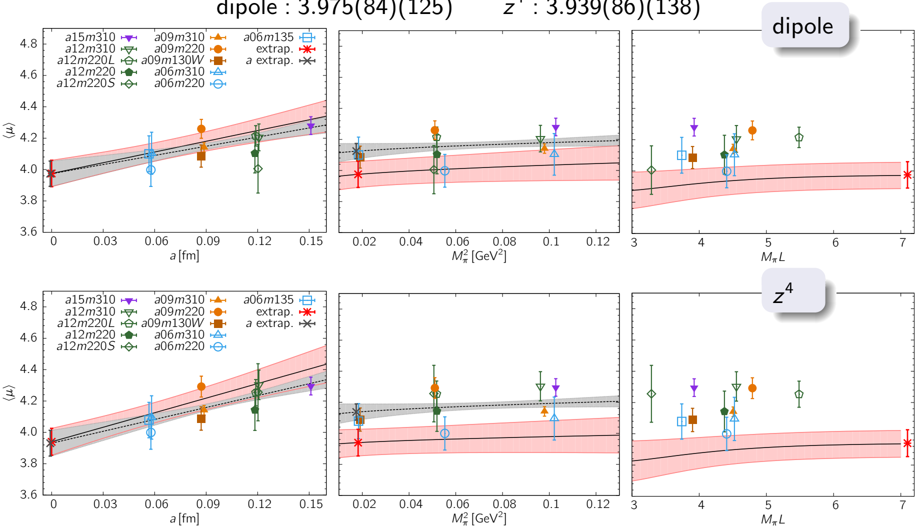

Summary (2)

- We analyzed 11 ensembles of $2+1+1$-flavor HISQ sea quarks with clover valence quark. ($a \approx 0.06, 0.09, 0.12, 0.15\,\mathrm{fm}$, $M_\pi \approx 135, 220, 310\,\mathrm{MeV}$, $3.3 \lesssim M_\pi L \lesssim 5.5$)
- With high statistics of $\mathcal{O}(10^5)$, we can address various systematics (ESC, scale setting, CCFV and kinematic extrapolations) in form factor calculations.
- The weak unitarity constraint is crucial to stabilize the z-expansion.
- z-expansion results are consistent with the dipole fit, but the errors are 2–3 times larger.
- The extraction of $\langle r_E^2 \rangle$, $\langle r_M^2 \rangle$, μ could have $\mathcal{O}(10\%)$ errors due to each (1) statistics and ESC, and (2) parameterization of Q^2 behavior.
- We do not consider the smaller values of $\langle r_E^2 \rangle, \langle r_M^2 \rangle, \mu$ implies a significant deviations from the experimental values.
- Data points at smaller $Q^2 < 0.1\mathrm{GeV}^2$ are highly desirable in future calculations.

	$\langle r_E^2 \rangle$ (fm^2)	$\sqrt{\langle r_E^2 \rangle}$ (fm)	$\langle r_M^2 \rangle$ (fm^2)	$\sqrt{\langle r_M^2 \rangle}$ (fm)	μ (Bohr Magneton)
dipole fit	0.586(17)(13)	0.765(11)(8)	0.495(29)(41)	0.704(21)(29)	3.975(84)(125)
z^4 fit	0.591(41)(46)	0.769(27)(30)	0.450(65)(102)	0.671(48)(76)	3.939(86)(138)
Combined fit	0.564(114)	0.751(76)	0.459(189)	0.678(140)	3.922(83)

$$\sqrt{\langle r_E^2 \rangle}|_{\rm exp}=0.929(27)\ \mathrm{fm}\ , \quad \sqrt{\langle r_M^2 \rangle}|_{\rm exp}= 0.849(11)\ \mathrm{fm}$$

$$\mu|_{\rm exp}=4.7058 = 1+\kappa_p-\kappa_n\ , \quad \kappa_p = 1.79284735(1)\ , \ \ \kappa_n = -1.91304273(45)$$

Thank you for your attention.

Nucleon Structure, Proton Radius

- $e - p$ scattering, H laser spectroscopy $\quad r_{E,p} = 0.875(6)\,\mathrm{fm}$
  [CODATA2014 RMP **88**, 035009 (2016)]
- muonic hydrogen laser spectroscopy $\quad r_{E,p} = 0.8409(4)\,\mathrm{fm}$
  [R. Pohl *et.al.*, Nature **466**, 213 (2010)]
  [A. Antognini *et al.*, Science **339**, 417 (2013)]
- Lattice QCD
- New Physics (?)

Controlling Excited States: multistates fits

$$C^{2\text{pt}}(t, \boldsymbol{p}) = |\mathcal{A}_0|^2 e^{-E_0 t} + |\mathcal{A}_1|^2 e^{-E_1 t} + |\mathcal{A}_2|^2 e^{-E_2 t} + |\mathcal{A}_3|^2 e^{-E_3 t} + \cdots$$

- 2-state fit $\rightarrow$ 4-state fit
- The lowest three states Energies and $\mathcal{A}$mplitudes are feed into 3-pt correlator analysis.
- plot effective mass from fits and data $E_{\text{eff}}(t) = \log \frac{C^{2\text{pt}}(t)}{C^{2\text{pt}}(t+1)} \rightarrow E_0$

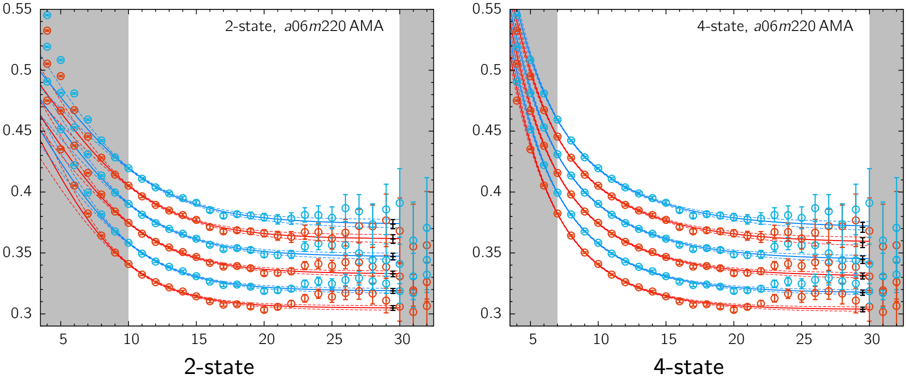

Controlling Excited States: different smearing size

- Covariant gaussian smearing: $\left[1 + \sigma^2 \nabla^2 / (4N)\right]^N$
- 4-state fit, $\boldsymbol{p} = 0$

$$C^{2\text{pt}}(t, \boldsymbol{p}) = |\mathcal{A}_0|^2 e^{-M_0 t} + |\mathcal{A}_1|^2 e^{-M_1 t} + |\mathcal{A}_2|^2 e^{-M_2 t} + |\mathcal{A}_3|^2 e^{-M_3 t} + \cdots$$

- Larger size of smearing radius improves an overlap with the ground state
  $\rightarrow$ plateau appears from earlier t
- At large t, the correlator become noisier

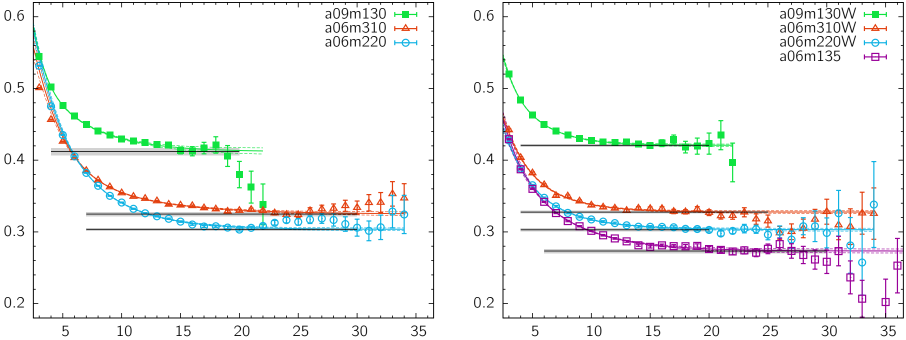

$\sigma = 5.5, 6.5, 5.5$ $\qquad$ $\sigma = 7, 12, 11, 9$

Extracting Form Factors from 3-pt Correlaotrs

- Matrix elements $\langle m'|\mathcal{O}_\Gamma|n\rangle$ are extracted from a simultaneous fit to the correlator $C_\Gamma^{(3pt)}$ calculated at multiple source and sink separation τ.

$$\begin{aligned}
C_\Gamma^{(3pt)}(t;\tau;\boldsymbol{p}',\boldsymbol{p}=\boldsymbol{0}) &= |\mathcal{A}_0'||\mathcal{A}_0|\langle 0'|\mathcal{O}_\Gamma|0\rangle e^{-E_0 t - M_0(\tau - t)} \\
&+ |\mathcal{A}_1'||\mathcal{A}_1|\langle 1'|\mathcal{O}_\Gamma|1\rangle e^{-E_1 t - M_1(\tau - t)} + |\mathcal{A}_2'||\mathcal{A}_2|\langle 2'|\mathcal{O}_\Gamma|2\rangle e^{-E_2 t - M_2(\tau - t)} \\
&+ |\mathcal{A}_0'||\mathcal{A}_1|\langle 0'|\mathcal{O}_\Gamma|1\rangle e^{-E_0 t - M_1(\tau - t)} + |\mathcal{A}_1'||\mathcal{A}_0|\langle 1'|\mathcal{O}_\Gamma|0\rangle e^{-E_1 t - M_0(\tau - t)} \\
&+ |\mathcal{A}_0'||\mathcal{A}_2|\langle 0'|\mathcal{O}_\Gamma|2\rangle e^{-E_0 t - M_2(\tau - t)} + |\mathcal{A}_2'||\mathcal{A}_0|\langle 2'|\mathcal{O}_\Gamma|0\rangle e^{-E_2 t - M_0(\tau - t)} \\
&+ |\mathcal{A}_1'||\mathcal{A}_2|\langle 1'|\mathcal{O}_\Gamma|2\rangle e^{-E_1 t - M_2(\tau - t)} + |\mathcal{A}_2'||\mathcal{A}_1|\langle 2'|\mathcal{O}_\Gamma|1\rangle e^{-E_2 t - M_1(\tau - t)} + \cdots
\end{aligned}$$

- $\langle 2'|\mathcal{O}_\Gamma|2\rangle = 0$

- Decompose the ground state matrix elements

$$\langle 0'|\mathcal{O}_\Gamma|0\rangle = K_{E,\Gamma} G_E(Q^2) + K_{M,\Gamma} G_M(Q^2)$$

- Data is displayed using the following ratio.

$$\mathcal{R}_\Gamma(t,\tau,\boldsymbol{p}',\boldsymbol{p}) = \frac{C_\Gamma^{(3pt)}(t,\tau;\boldsymbol{p}',\boldsymbol{p})}{C^{(2pt)}(\tau,\boldsymbol{p})} \times \left[\frac{C^{(2pt)}(t,\boldsymbol{p})C^{(2pt)}(\tau,\boldsymbol{p})C^{(2pt)}(\tau - t,\boldsymbol{p}')}{C^{(2pt)}(t,\boldsymbol{p}')C^{(2pt)}(\tau,\boldsymbol{p}')C^{(2pt)}(\tau - t,\boldsymbol{p})}\right]^{1/2} \underset{\substack{\tau \to \infty \\ 0 \ll t,\tau - t}}{\longrightarrow} \langle 0'|\mathcal{O}_\Gamma|0\rangle$$

Extraction of G_E

- $\mathrm{Im}\, C[V_i] \to K q_i G_E$, $K = 1/\sqrt{2E(E+M)}$
- $\mathrm{Re}\, C[V_4] \to K(E+M) G_E$
- Two channels result in systematically different G_E mostly for small $Q^2 \lesssim 0.2$, where the charge radius is sensitive.

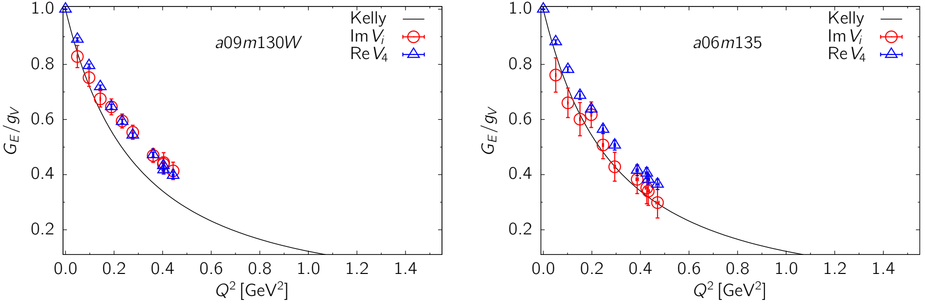

Extraction of G_E

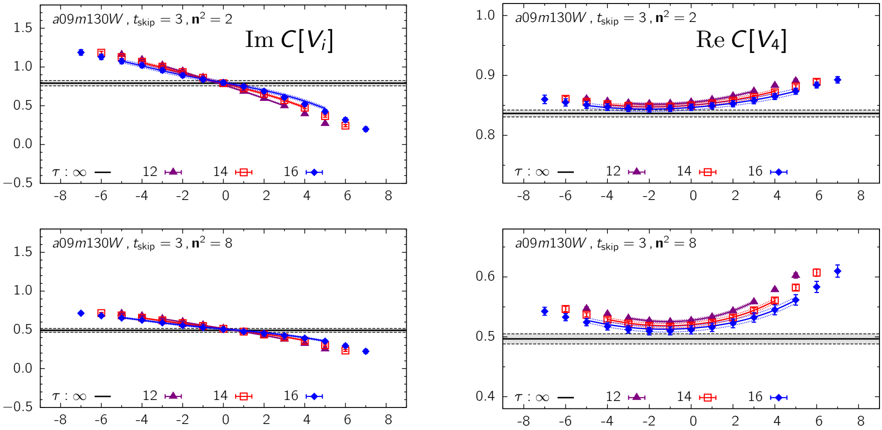

- Excited states contaminations to $\mathrm{Im}\, C[V_i]$ and $\mathrm{Re}\, C[V_4]$ are very different.
- a larger excited state effect in $\mathrm{Im}\, C[V_i]$ for a small momentum (top: $\boldsymbol{n}^2 = 2$)
- $G_E(0)$ is not accessible to $\mathrm{Im}\, C[V_i]$.
- We use G_E from $\mathrm{Re}\, C[V_4]$.

z-expansion: Experimental Data

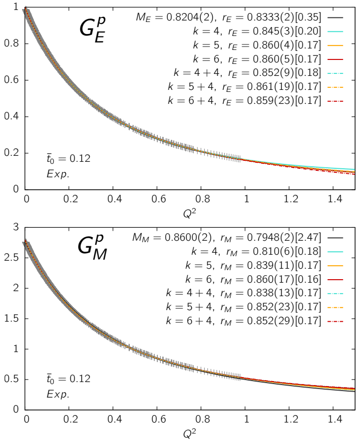

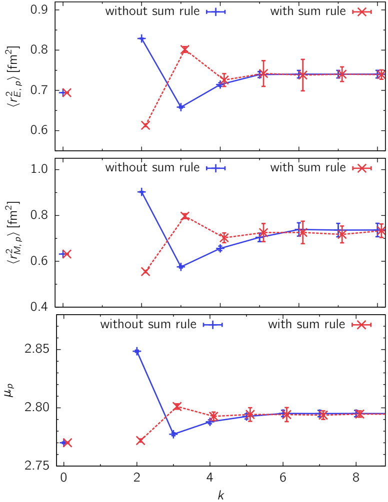

[rebinned experimental data, D. Higinbotham]

- z-expansion converges for $k \geq 5$
- fits with/without sum rules converges to the same value

Comparison with Other Near Physical Pion Mass Calculations

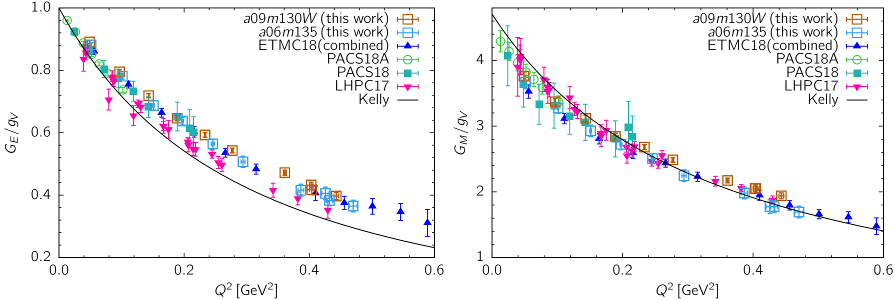

- For $Q^2 < 0.2\,\mathrm{GeV}^2$, G_E (G_M) from lattice calculations approaches the Kelly parameterization of experimental data from above (below).
- PACS'18 and LHPC'17 data are consistent with the rest, but the errors are larger.
- All the PACS'18A data are at $Q^2 < 0.1\,\mathrm{GeV}^2$ and show better agreement with the Kelly curve.

Comparison with Other Near Physical Pion Mass Calculations

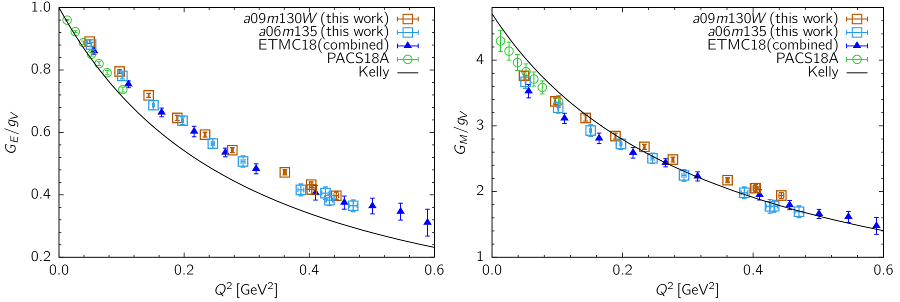

	a [fm]	M_π [MeV]	$L^3 \times T$	$M_\pi^{\rm val} L$	τ/a	$N_{\rm conf}$	$N_{\rm meas}$	Action
$a09m130W$	0.0871(6)	138.1(1.0)	$64^3 \times 96$	3.90	$\{8,10,12,14,16\}$	1290	165,120	2+1+1 HISQ
$a06m135$	0.0570(1)	135.6(1.4)	$96^3 \times 192$	3.7	$\{16,18,20,22\}$	675	43,200	+ Clover
ETMC'18	0.0809(4)	138(1)	$64^3 \times 128$	3.62	$\{12,14,16,18,20\}$	750	3K–48K	2+1+1 TM
ETMC'18	0.0938(3)	130(2)	$64^3 \times 128$	3.97	$\{12,14,16\}$	330–1040	5K–17K	2 TM
PACS'18A	0.0846(7)	146	$96^3 \times 96$	6.01	$\{15\}$	200	12,800	2+1 Clover
PACS'18	0.0846(7)	135	$128^3 \times 128$	7.41	$\{10,12,14,16\}$	20	2.5K–10K	2+1 Clover
LHPC'17	0.093	135	$64^3 \times 64$	4.08	$\{10,13,16\}$	442	56,576	2+1 Clover

- All the PACS'18A data are at $Q^2 < 0.1\,\mathrm{GeV}^2$ and show better agreement with the Kelly curve. Further calculations with multiple lattice spacings, larger Q^2 points, higher statistics are interesting.

Axial Form Factors G_A and Charge Radius $\langle r_A^2 \rangle$

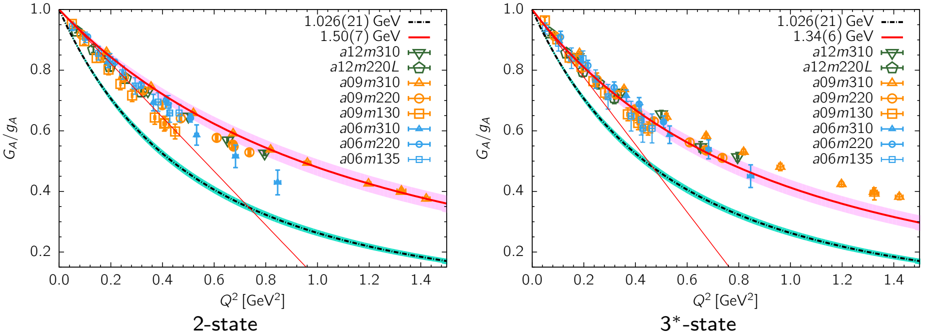

3-state analysis results in a larger $\langle r_A^2 \rangle$.

$\Rightarrow$ Data from two physical ensembles become close.

$\Rightarrow$ The physical limit still shows large deviation from the experimental data.

Controlling Excited State Contribution to G_A, $\widetilde{G}_P$, G_P

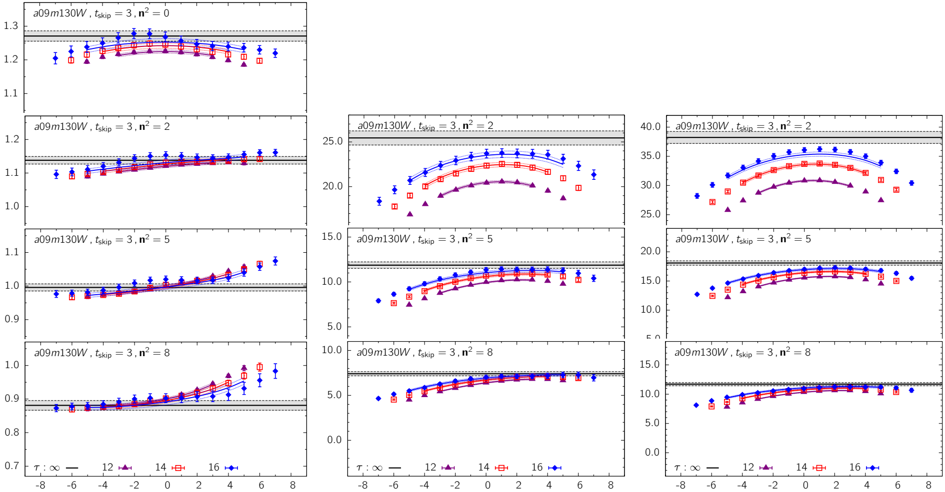

$\mathrm{Im}\,\mathcal{R}_{53}, q_3 = 0 \rightarrow G_A(Q^2)$ $\mathrm{Im}\,\mathcal{R}_{51} \rightarrow \widetilde{G}_P(Q^2)$ $\mathrm{Re}\,\mathcal{R}_5 \rightarrow G_P(Q^2)$

Very similar Excited State Contamination in $\widetilde{G}_P$ and G_P